An inverse approach integrating flowmeter and pumping test data for three-dimensional aquifer characterization

Mohammed Aliouache, Xiaoguang Wang, Pierre Fischer, Gerard Massonnat, Herve Jourde

An inverse approach integrating flowmeter and pumping test data for three-dimensional aquifer characterization

Mohammed Aliouache[a], Xiaoguang Wang[a,b,*], Pierre Fischer[a], Gerard Massonnat[c], Herve Jourde[a]

[a] *Laboratories Hydrosciences Montpellier, UMR 5151 CNRS-UM-IRD, Montpellier, France, 34000*

[b] *Chengdu University of Technology, Sichuan, China, 610059*

[c] *CSTJF-PAU Total Energies, Avenue Larribau, Pau, France, 64000*

*Correspondence: Xiaoguang Wang (wangxiaoguang@cdut.edu.cn, xiaoguang.wang@umontpellier.fr)

Highlights

1. Coupling flowmeter and pumping test data for low-cost 3D aquifer characterizations
2. 3D hydraulic conductivity distribution is assessed from an inverse approach
3. The effectiveness of integrating the two datasets is studied with 3D synthetic models

Abstract

The accurate characterization of the underground depositional structure and hydraulic property distribution is essential to understand flow and solute transport in heterogeneous rocks or soils. Hydraulic tomography was shown to be an efficient technique to infer the spatial distribution of hydraulic properties. Due to the fact that information about the sedimentary structures' distribution is not always available to allow a three-dimensional characterization, many of existing field applications of hydraulic tomography have been limited to two-dimensional imaging along horizontal layer or vertical profiles where hydraulic data were collected.

In this work, we explore the potential of combining tomographic pumping and flowmeter tests responses in an inverse approach for three-dimensional aquifer characterization. The tomographic pumping data provide information about the lateral hydraulic connections between boreholes, while the flowmeter data constrain the vertical heterogeneity structure. The inverse approach is first validated using two synthetics models composed of multi-layered depositional structures and heterogeneous hydraulic properties within each layer. It is shown that adding the information provided by the flowmeter profiles, the inverted model exhibits more realistic depositional features. We then apply the proposed approach to characterize the 3D hydraulic conductivity field controlled by sedimentary structure of an experimental site in layered porous rocks. The inverted hydraulic conductivity field is in a good agreement with permeability measurement on drilled cores. The proposed method offers an efficient and low-cost approach for rapid assessment of the hydraulic properties in 3D and could be extrapolated to other field applications.

1. Introduction

The characterization of hydraulic properties, such as hydraulic conductivity and specific storage, is very important in groundwater modeling and water resources management (Hubbard and Rubin, 2005). Contaminant transport has always been strongly dependent on the accuracy of the hydraulic properties' characterization. A minor change in hydraulic properties may alter transport behaviors significantly (Zheng and Gorelick, 2003). Because direct measurements of hydraulic properties are limited in real-world applications, early analytical analysis of aquifer hydraulic response to pumping/injection often adopts a homogeneous assumption (e.g., Theis 1935, Cooper and Jacob 1946). It may be enough to infer the bulk aquifer property; however, it cannot capture most of the transient behavior of the tested aquifer. In addition to pumping tests, several other hydraulic testing methods, such as slug tests (Yeh et al., 1995) and flowmeter tests (Rehfeldt et al., 1992, Klepikova et al., 2013, Tamayo-Mas et al., 2018), are being used to provide non-redundant information (with respect to pumping tests) about the aquifer.

Hydraulic tomography (HT) has been developed over the last two decades (e.g., Gottlieb and Dietrich, 1995, Butler et al., 1999, Bohling et al., 2002, Bohling and Butler, 2010, Yeh and Liu, 2000, Zhu and Yeh, 2005, Zhu and Yeh, 2006, Liu et al., 2002, Liu et al., 2007, Illman et al., 2010, Cardiff et al., 2009, Zha et al. 2014). This approach has shown a great potential for reconstructing detailed spatial distributions of hydraulic parameters comparing to the traditional analytical solutions. Hydraulic tomography yields a detailed two- or three-dimensional map of hydraulic heterogeneity for regions within between the testing boreholes where constraining hydraulic head responses to cross-hole pumping are collected. The efficiency of HT has been demonstrated in many laboratory-scale (e.g., Liu et al., 2007, Illman et al., 2007, Illman et al., 2010, Zhao et al., 2016, Zhao and Illman 2017) and field-scale studies (e.g., Bohling et al., 2007, Brauchler et al., 2011, Brauchler et al., 2013, Berg and Illman, 2011, Cardiff et al., 2012, Fischer et al., 2020).

For a full 3D hydraulic tomography, using only one observation from each testing well is not sufficient and packer tests are often required (Bholing et al. 2007, Berg and Illman 2011, Zha et al.

2016, Zha et al. 2017, Cardiff et al. 2012, Zhao and Illman 2017, Wen et al. 2020). However, packer tests, which are costly and complex to set up, are not always available in each experiment site. Without packer tests, pumping tests data remain insufficient to capture the three-dimensional aquifer behavior and may lead to erroneous characterization and sometimes model instability in layered aquifers.

In recent years, other information such as geological and geophysical data have been used to constrain the inverse process of HT (e.g., Zha et al. 2017, Tso et al. 2016, Soueid Ahmed et al. 2015). The most widely-used geostatistics-based inverse modelling approaches are the quasi-linear geostatistical approach (Kitanidis 1995) and the successive linear estimator (SLE) (Yeh et al. 1996). To improve efficiency when dealing with highly parameterized inverse problems, different approaches were developed, including principle component geostatistical approach (Kitanidis and Lee 2014), reduced-order SLE (Zha et al. 2018) and the use of geostatistical reduced order models (Liu et al. 2013). Previous works have highlighted the benefits of incorporating site-specific geologic structure information into groundwater models when HT data are limited (Zha et al. 2017, Tso et al. 2016). Zha et al. (2017) worked on quantitative incorporation of site-specific information into groundwater models and introduced a general method to derive conditional mean and conditional covariance, that can be used in HT analysis as prior information. Tso et al. (2016) also concluded that only incorporating a qualitative facies trend information already yields a better conductivity estimate. Such improvement can also be seen in hydraulic conductivity estimates through laboratory/ field applications (Zhao et al. 2016, Zhao and Illman 2017). De Clercq et al. (2020) used electrical resistivity maps to structure the distribution of the hydraulic properties in a 3D HT.

Flowmeter surveys characterize the vertical inflow profile of a given well (Paillet et al. 1998, Molz et al. 1994, Zlotnik and Zurbuchen 2003, Williams and Paillet. 2002, Day-Lewis et al. 2011). They are a widely used approach to determine vertical profiles of hydraulic conductivities at well locations. Complex geological medias are often layered systems and flowmeter analysis has shown its efficiency to detect the main layers contributing to the total pumped flux (Day-Lewis et al. 2011, Paillet and Reese 2000). Flowmeter profiling can also be used to detect the well crossing fractures that contribute

87 to flow (Day-Lewis et al. 2011, Roubinet et al. 2015). Flowmeter tests are easy and cheap but bulky
88 and the investigated height is limited due to the space taken by the pump and the generated drawdown.
89 Flowmeter tests may provide a new set of information and have been included in inverse modelling
90 problems. For instance, Fienen et al. (2004) used a Bayesian inverse approach to interpret the vertical
91 hydraulic conductivity in a heterogeneous fractured aquifer. Other applications used the interpreted
92 hydraulic conductivity values from flowmeter tests in the transmissivity map to constrain the
93 geostatistical inversions (e.g., Rehfeldt et al. 1992; Chen et al. 2001). In other studies, flux
94 measurements have also been used as observation data additional to hydraulic heads in hydraulic
95 tomography (Li et al. 2008, Zha et al. 2014, Tso et al. 2016).

96 Combining different hydraulic tests that characterize different parts of the aquifer may lead into a
97 good characterization; for example, combining flowmeter tests data that give vertical information with
98 pumping tests data that give lateral information might be a good alternative to obtain a three-
99 dimensional characterization of the aquifer without packer tests. In this paper, we integrate vertical
100 hydrogeological information obtained from flowmeter surveys and horizontal information from cross-
101 hole pumping tests to achieve a 3D transient hydraulic tomographic (THT) characterization of
102 sedimentary layered rocks. The flowmeter data are incorporated to HT through the construction of
103 conditional initial mean and covariance of model parameter. We first validate the proposed inversion
104 framework using synthetic data from a two-dimensional cross-section model and a three-dimensional
105 model. We then apply the inverse approach to a real-world study in an experimental site composed of
106 layered porous rocks. In the end, we analyze the data fitting effectiveness and geological coherence of
107 the inverted hydraulic conductivity fields.

108 ## 2. Methodology

109 The objective of the study is to integrate two sets of data to obtain spatialized hydraulic conductivity
110 estimates through hydraulic tomography. The first dataset corresponds to drawdown responses to
111 pumping tests that give information about lateral variation of hydraulic properties. The second dataset
112 consists in flowmeter logs measured in every well of the site that give vertical information (see Figure

1 for datasets scheme). Flowmeter logs are first interpreted and converted into hydraulic conductivity profiles. Then, the interpreted hydraulic conductivity profiles are interpolated using a triangular-base bilinear or trilinear interpolation in order to obtain a continuous two- or three-dimensional hydraulic conductivity map between the wells and we use 'nearest neighbors' interpolation for the rest of the inversion domain where the linear interpolation cannot be evaluated. After that, an inverse modelling approach is used to reconstruct the hydraulic conductivity distribution using interpolated map as a prior information. We use the principal component geostatistical approach, a deterministic iterative procedure that updates the conditional mean and the conditional covariance by matching model responses to the pumping tests observations.

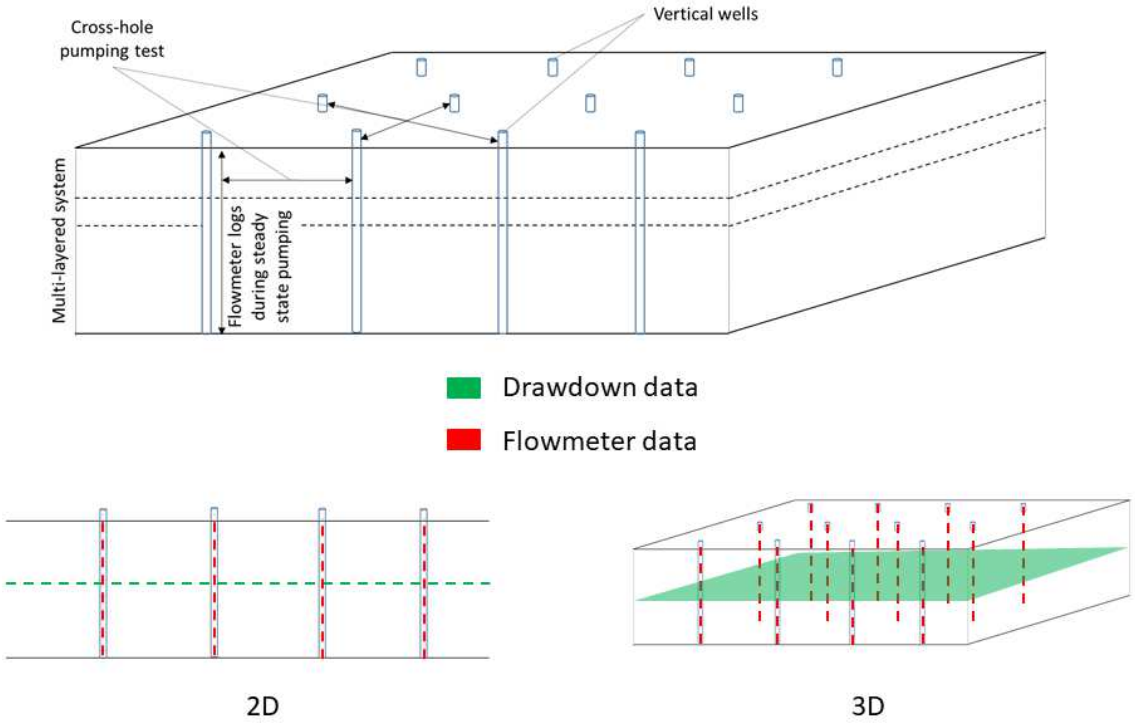

Figure 1*: Data usage scheme. Red dashes correspond to flowmeter log data and green surface corresponds to cross-hole pumping tests data. The wells are open hole and the drawdowns are sampled at the green z-level.*

2.1 Groundwater flow model

We solve the problem of three-dimensional transient fluid flow through a confined, saturated and heterogeneous porous media. The system is solved in transient regime and is described by the following equations:

$$\boldsymbol{S_s \frac{\partial h}{\partial t} + \nabla(-K \nabla h) = Q,} \quad \textbf{(1)}$$

with

$$\boldsymbol{h|_{t=0} = h_0, h|_{\varphi} = h_0,} \quad \textbf{(2)}$$

where ∇ is the gradient operator, S_s is the specific storage which assumed constant in this study, h is the hydraulic head, K the hydraulic conductivity, Q the source term and h_0 is the initial hydraulic head which remains constant at the boundary conditions $\boldsymbol{\varphi}$. The forward flow model is solved using a finite element method using unstructured mesh (See Figure R3 in supplementary materials).

2.2 Flowmeter analysis

The applied approach of flowmeter data analyses is described in Molz et al. (1989), which is based on the study of flow in a layered, stratified aquifer by Javandel and Witherspoon (1969). Assuming that the idealized aquifer is layered and the flow quickly becomes horizontal even with high contrast of hydraulic conductivity between the layers. The flow of a given layer is proportional to the hydraulic conductivity of that layer and the sum of the different flow rates into the well is equal to the pump flow rate during the pumping test.

During our flowmeter test, water is extracted from an open hole well and, once steady state is reached, a spinner flowmeter is swept along the well from the bottom of the well to the top and a vertical flow rate profile is measured. In most common cases, when the pump is located at the top, the flow rate log will have the trend of an increasing curve starting from a zero value at the bottom to a max value at the top, that will correspond to the total extracted flux from the well. The increase in flow rate over a certain depth increment is correlated to the relative hydraulic conductivity profile; higher the hydraulic conductivity, stronger the rate increase. Flowmeter tests therefore provide relative values of

hydraulic conductivity distribution along the borehole. In order to extract the absolute values, an effective value of hydraulic conductivity of the well (obtainable from the interpretation single hole of a pumping tests) will be used. Single-hole flowmeter data can be analyzed to estimate conductivity profiles along boreholes and characterize aquifer compartmentalization (Molz et al. 1989; Kabala 1994; Paillet et al. 1998).

If a well is subject to a pumping with a pump placed at the top of the well working at the rate Q_p, the underground layers connected to that well will contribute to the total extracted flux. Their contribution is proportional to their hydraulic conductivity. For the following equations, b (m) refers to the aquifer thickness, z_0 (m) the reference level of the borehole bottom, and z (m) the height above the bottom (Figure 2). In an idealized layered aquifer, the flow into the well from a given layer is proportional to the transmissivity of that layer:

$$\Delta \boldsymbol{Q_i} = \boldsymbol{\alpha} \Delta \boldsymbol{z_i} \boldsymbol{K_i} \, , \tag{3}$$

where α (m) is a constant of proportionality, ΔQ_i (m^3/s) corresponds to the induced flow increments observed in the borehole along the i^{th} increment of height Δz_i (m) that has a hydraulic conductivity K_i (m/s). The average horizontal hydraulic conductivity K_{avg} can be expressed by:

$$\boldsymbol{K_{avg}} = \frac{\sum \boldsymbol{K_i} \Delta \boldsymbol{z_i}}{\boldsymbol{b}} . \tag{4}$$

The cumulative flow $Q_{cum}(b)$ over the aquifer thickness can be expressed as follows:

$$\boldsymbol{Qcum(b)} = \int_{\boldsymbol{z0}}^{\boldsymbol{b}} \boldsymbol{Q(z)dz} \; = \boldsymbol{Q_p} = \sum_{\boldsymbol{i}} \Delta \boldsymbol{Q_i} = \boldsymbol{\alpha} \sum_{\boldsymbol{i}} \Delta \boldsymbol{z_i} \boldsymbol{K_i} = \boldsymbol{\alpha} \boldsymbol{K_{avg}} \boldsymbol{b} \; . \tag{5}$$

By substituting the sum, α can be solved as:

$$\boldsymbol{\alpha} = \frac{\boldsymbol{Q_p}}{\boldsymbol{K_{avg}} \boldsymbol{b}} . \tag{6}$$

Then, the hydraulic conductivity of each layer can be quantified by:

$$K_i = \frac{\Delta Q_i K_{avg} b}{Q_p \Delta z_i} \quad . \tag{7}$$

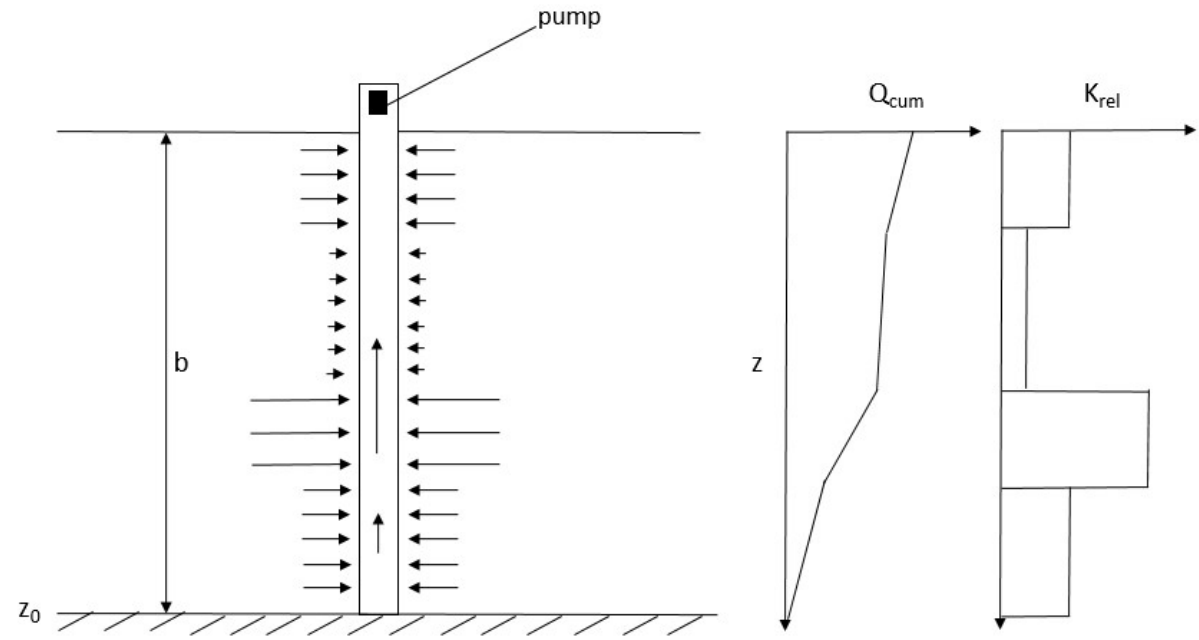

Figure 2*: Flowmeter setup scheme with an interpretation example. Qcum is the cumulative flow rate and Krel is the interpreted relative permeability from flow log.*

2.2 Principal component geostatistical approach

In order to optimize the hydraulic conductivity field in the model we use the principal component geostatistical approach (PCGA) (Kitanidis and Lee 2014). The observation equation that links the *m* unknown hydraulic conductivities, stored in a vector **s,** to the observation data (hydraulic heads) stored in a matrix **y** is (Kitanidis 1995):

$$\boldsymbol{y} = \boldsymbol{h}(\boldsymbol{s}) + \boldsymbol{v}, \tag{8}$$

where $\boldsymbol{h}()$ is the forward model, $\boldsymbol{v}$ is the observation error with a random normal distribution with mean 0 and variance **R**, which is usually the error measurement multiplied by the identity matrix. The prior probability of $\boldsymbol{s}$ is a Gaussian distribution with mean $\boldsymbol{X\beta}$ generalized by a covariance matrix $\boldsymbol{Q}$. **X** is a *m*-vector of ones and $\boldsymbol{\beta}$ represents the mean hydraulic conductivity value. The posterior probability density function (objective function **L**) of $\boldsymbol{s}$ and $\boldsymbol{\beta}$ is given by:

$$\mathbf{L} = \frac{1}{2}\left(\boldsymbol{y} - \boldsymbol{h}(\boldsymbol{s})\right)^{\boldsymbol{T}} \boldsymbol{R}^{-1}\left(\boldsymbol{y} - \boldsymbol{h}(\boldsymbol{s})\right) + \frac{1}{2}(\boldsymbol{s} - \boldsymbol{X\beta})^{\boldsymbol{T}} \boldsymbol{Q}^{-1}(\boldsymbol{s} - \boldsymbol{X\beta})\,. \quad \textbf{(9)}$$

The optimization of the hydraulic conductivity values is obtained by minimizing this objective function through an iterative method.

Inversion process requires the calculation of the sensitivity matrix (Jacobian matrix) which require as much forward model simulations as unknowns *m*. Despite the computer science advancement, the forward model itself can be time consuming when dealing with high dimensional problems (3D simulations, fine mesh, presence of complex structures). In order to bypass this difficulty, the principal component geostatistical approach which avoids the full Jacobian matrix calculation, was proposed. The reduced order successive linear estimator ROSLE (Zha et al. 2018) based on SLE (Yeh, 1996) can be one alternative to the PCGA. These methods use a singular value decomposition and then a truncation based on the eigenvalues and Eigen functions of the covariance matrix $\boldsymbol{Q}$. The covariance matrix can be rewritten with its decomposed form as:

$$\boldsymbol{Q} = \boldsymbol{VSV^T}\,, \quad \textbf{(10)}$$

where **V**'s columns correspond to the eigenvectors of the covariance matrix and **S** is a diagonal matrix of its eigenvalues **λ** which are decreasingly organized. The eigenvectors and eigenvalues are then **k**-rank truncated. The **k** first eigenvalues and its corresponding eigenvectors are kept. The compressed covariance can be calculated as:

$$\boldsymbol{Q_k} = \boldsymbol{V_k S_k V_k^T}\,, \quad \textbf{(11)}$$

where

$$\boldsymbol{Q_k} \approx \boldsymbol{Q}\,, \quad \textbf{(12)}$$

It can be also written as a sum:

$$\boldsymbol{Q_k} = \boldsymbol{V_k S_k V_k^T} = \sum_{i=1}^{k} \boldsymbol{\xi_i \xi_i^T}, \quad \textbf{(13)}$$

where

$$\boldsymbol{\xi_i} = \sqrt{\boldsymbol{\lambda_i}}\boldsymbol{V_i}. \tag{14}$$

The accuracy of the low-rank covariance depends on the truncation number. However, it is already shown that a much smaller truncation number than the number of unknowns (**k**<<*m)* can be used (Kitanidis and Lee, 2014). The quasi-Linear geostatistical approach (Kitanidis, 1995) updates the actual best estimate $\bar{\boldsymbol{s}}$ for the next iteration as:

$$\bar{\boldsymbol{s}} = \boldsymbol{X}\bar{\boldsymbol{\beta}} + \boldsymbol{Q}\boldsymbol{H}^{\boldsymbol{T}}\bar{\boldsymbol{\xi}}\,, \tag{15}$$

where **H** is the Jacobian matrix and the accentuation-bar denotes the best estimate. $\bar{\boldsymbol{\beta}}$ and $\bar{\boldsymbol{\xi}}$ are solved from the following linear system:

$$\begin{bmatrix} \boldsymbol{H}\boldsymbol{Q}\boldsymbol{H}^{\boldsymbol{T}} + \boldsymbol{R} & \boldsymbol{H}\boldsymbol{X} \\ (\boldsymbol{H}\boldsymbol{X})^{\boldsymbol{T}} & \mathbf{0} \end{bmatrix} \begin{bmatrix} \bar{\boldsymbol{\xi}} \\ \bar{\boldsymbol{\beta}} \end{bmatrix} = \begin{bmatrix} \boldsymbol{y} - \boldsymbol{h}(\bar{\boldsymbol{s}}) + \boldsymbol{H}\bar{\boldsymbol{s}} \\ \mathbf{0} \end{bmatrix}. \tag{16}$$

The minimized objective function **L** can also be written as:

$$\boldsymbol{L} = \frac{\mathbf{1}}{\mathbf{2}}\left(\boldsymbol{y} - \boldsymbol{h}\left(\boldsymbol{X}\boldsymbol{\beta} + \boldsymbol{Q}\boldsymbol{H}^{\boldsymbol{T}}\boldsymbol{\xi}\right)\right)^{\boldsymbol{T}} \boldsymbol{R}^{-\mathbf{1}} \left(\boldsymbol{y} - \boldsymbol{h}\left(\boldsymbol{X}\boldsymbol{\beta} + \boldsymbol{Q}\boldsymbol{H}^{\boldsymbol{T}}\boldsymbol{\xi}\right)\right) + \frac{\mathbf{1}}{\mathbf{2}}\boldsymbol{\xi}^{\boldsymbol{T}}\boldsymbol{H}\boldsymbol{Q}\boldsymbol{H}^{\boldsymbol{T}}\boldsymbol{\xi}. \tag{17}$$

In PCGA, the sensitivity matrix **H** is not fully calculated and an alternative way to approximate it is proposed.

In order to estimate **HQ** and $\mathbf{HQH^T}$, **k** forward runs are needed to be solved in additional to the forward run of the actual best estimate, the forward models are used to calculate **η** defined as follows:

$$\boldsymbol{\eta_i} = \boldsymbol{H}\boldsymbol{\xi_i} \approx \frac{\mathbf{1}}{\boldsymbol{\delta}}[\boldsymbol{h}(\boldsymbol{s} + \boldsymbol{\delta}\boldsymbol{\xi_i}) - \boldsymbol{h}(\boldsymbol{s})], \tag{18}$$

δ is the finite difference interval from the Taylor series expansion (Kitanidis and Lee, 2014). Then **HQ** and $\mathbf{HQH^T}$ are defined as:

$$\boldsymbol{H}\boldsymbol{Q} \approx \boldsymbol{H}\boldsymbol{Q}_{\boldsymbol{k}} = \boldsymbol{H}\sum_{\boldsymbol{i}=\mathbf{1}}^{\boldsymbol{k}} \boldsymbol{\xi}_{\boldsymbol{i}}\,\boldsymbol{\xi}_{\boldsymbol{i}}^{\boldsymbol{T}} = \sum_{\boldsymbol{i}=\mathbf{1}}^{\boldsymbol{k}} (\boldsymbol{H}\boldsymbol{\xi}_{\boldsymbol{i}})\,\boldsymbol{\xi}_{\boldsymbol{i}}^{\boldsymbol{T}} = \sum_{\boldsymbol{i}=\mathbf{1}}^{\boldsymbol{k}} \boldsymbol{\eta}_{\boldsymbol{i}}\,\boldsymbol{\xi}_{\boldsymbol{i}}^{\boldsymbol{T}}, \tag{19}$$

$$\boldsymbol{HQH^T \approx HQ_kH^T = H[\sum_{i=1}^{k} \xi_i \xi_i^T]H^T = \sum_{i=1}^{k}(H\xi_i)(H\xi_i)^T = \sum_{i=1}^{k} \eta_i \eta_i^T.} \quad \textbf{(20)}$$

In order to estimate **HX**, one (columns of **X**) forward run is needed, following:

$$\boldsymbol{HX_i \approx \frac{1}{\delta}[h(\bar{s} + \delta X_i) - h(\bar{s})]\,.} \quad \textbf{(21)}$$

In order to estimate $\mathbf{H\bar{s}}$, one forward run is needed in addition to the forward model of the actual best estimate, following:

$$\boldsymbol{H\bar{s} = \frac{1}{\delta}[h(\bar{s} + \delta\bar{s}) - h(\bar{s})] + O(\delta) \approx \frac{1}{\delta}[h(\bar{s} + \delta\bar{s}) - h(\bar{s})].} \quad \textbf{(22)}$$

In total, each iteration requires **k+3** forward runs; 1 forward run of the actual best estimate, 1 forward run to estimate $\mathbf{H\bar{s}}$, 1 forward run to estimate **HX** and **k** forward models to estimate **HQ** and $\mathbf{HQH^T}$. The above steps are repeated iteratively until convergence of the objective function value is reached.

2.3 Prior information

The approach of conditional mean and conditional covariance using geological information as presented in Zha et al. (2017) work is used in this study. The two main prior information are the initial guess and the initial covariance matrix. The prior input of the inversion is constructed using interpreted flowmeter data. The 3D interpolated conductivity is mapped into inversion grid, stored in **s**, and used as an initial guess for the first iteration instead of using an initial mean.; an interpolation or/and an extrapolation might be often used. It also allows identifying the main facies and constructing the prior covariance accordingly (Zha et al. 2017). However, the covariance matrix **Q** is constructed as a sum of different covariance sub-matrixes (Zha et al., 2017): a) a covariance matrix that defines the different facies (layers) will be of high importance and its construction is achieved only by using a strong correlation between the cells that belong to the same facies, b) another covariance matrix that defines the correlation between the cells of the same facies, defined as an intra-facies covariance, c) a third covariance matrix, defined as an inter-facies covariance, can be used on the global inverted domain. By conditioning the prior covariance with facies information

252 distinguished from flowmeter data, we try to incorporate the vertical information into the inversion
253 process and constrain its convergence path.

254 ## 3. Validation of concept

255 The main objective of the paper is the use of two different datasets which are easily available to better
256 characterize the hydraulic conductivity of a multi-layered sedimentary structure constitutive of the
257 aquifer. The first dataset corresponds to flowmeter data along the profile of each well. Flowmeter logs
258 are obtained by pumping in the top of each well and the flowmeter tool is swept under the pump to get
259 the flow contribution along the borehole. The second dataset corresponds to measured hydraulic
260 response (drawdowns) to pumping tests. Here we try to perform a 3D inversion of the hydraulic
261 conductivity field to characterize the aquifer on the basis of pumping tests data and incorporating
262 flowmeter information. In order to validate this concept, the proposed inverse approach is first applied
263 on two synthetic cases. The first case is performed in 2D and the second one in 3D.

264 ### 3.1. 2D synthetic case

265 By using a two-dimensional random field generator tool (Paul Constantine 2021), a random hydraulic
266 conductivity field is generated following an exponential correlation function using the parameters of
267 standard deviation σ=1.5, the correlation length in x direction L_x=100 m, the correlation length in y
268 direction L_y=5 m. With such set of parameters, the obtained hydraulic conductivity field displays
269 multi-layered hydraulic properties (see Figure 3.a). We consider the obtained 2D map as a vertical
270 cross-section of an aquifer centered on the inverted domain which is extended using a buffer area until
271 the boundary conditions. The dimensions of the inverted domain are 70 m by 50 m; the dimensions of
272 the buffer area are 700 m by 50 m. The lateral boundaries are set to constant zero hydraulic head
273 while the upper and lower boundaries are set to no flow condition. The initial condition is set to zero
274 hydraulic head in the whole domain. For forward flow simulations, we use the subsurface flow
275 module of Comsol Multiphysics (COMSOL AB 2018). We assume the aquifer to be confined. The
276 specific storage is assumed constant and a value of $S_s = 10^{-4}$ m^{-1} was used.
277 The wells are modeled explicitly with a radius of r_w=0.1 m. We attribute to wells a high hydraulic
278 conductivity (K=1 m.s^{-1}) and a low specific storage (10^{-10} m^{-1}) (see Figure S1 in supplementary

material). The spacing of wells in the x direction is 15m (Figure 3a). We simulate five cross-hole pumping tests, which are considered as the 'data' for inversion. The location of selected wells is indicated in Figure S4. We simulate flowmeter data for each well by using a point source at the top of the well and applying a steady-state pumping flow rate. Once the steady-state flow regime is reached, we evaluate the vertical velocity along a line in the middle of the well. In our flow simulations, extra fine meshes are adopted to discretize the well domain (Figure R3). Examples of simulated flowmeter measurements for the 2D case can be found in supplementary material (Figure R2). For cross-hole pumping tests dataset to be used in HT, we simulate the transient hydraulic heads using a point source in the middle of explicitly modelled wells. The black dots shown in Figure 3 are the position of the points to be used as point source for the pumping tests and the monitoring points. For hydraulic head data, we sample at five different time steps covering the early to middle times for all pumping tests. The total number of drawdown data used for inversions are 5 (number of time steps) * 5 (number of pumping tests) * 4 (number of observation wells) = 100.

The simulated vertical velocity curves are converted into hydraulic conductivity distributions following the procedure described as follows (An example of the manipulation is provided in the supplementary information file).

- Step1：Discretize the vertical velocity profile into depth intervals Δz
- Step2：In each interval, evaluate the change in velocity Δv_i corresponding to the change in depth Δz_i
- Step3：Use Equation 7 to estimate K_i for each Δz_i
- Step4：Hydraulic conductivity profile is obtained in each well.

The hydraulic conductivity profiles are then interpolated using a triangular-base bilinear interpolation to obtain a hydraulic conductivity map for areas within between the wells. For the rest of the inversion domain where the linear interpolation cannot be evaluated, we use a nearest neighbors' extrapolation.

In the next step, we construct a nested covariance using the interpolated hydraulic conductivity map. The nested covariance is constructed by the combination of multiscale correlated heterogeneities (Zha et al. 2017). For example, a geological facies from another survey can be used a soft constraint added

306 into the initial covariance matrix for HT. The interface between different facies or zones may exhibit
307 an abrupt change of hydraulic properties. On the other hand, the variability inside a particular facies or
308 zone (compared to its large-scale mean) can be described by a zero mean and a small-scale covariance
309 function.
310 The covariance matrix used in HT of the 2D study is either calculated using a covariance model
311 similar to the one used to generate the true random field (Figures 3b and 3c), or built from a nested
312 covariance which is a sum of different covariance matrices: a covariance matrix built using a
313 covariance model similar to the one used to generate the true random field plus a covariance matrix
314 defining the important facies of flowmeter interpreted map (Figure 3e and 3f). The first covariance
315 matrix is simply calculated using an exponential covariance model with standard deviation=1.5,
316 correlation length in x direction L_x=100 m and correlation length in y direction L_y=5 m. For the
317 second covariance matrix that defines the facies, we simply identify the facies from flowmeter map
318 (Figure 3g) and we build a binary covariance that correlates the cells that belong to the same facies.
319 In the inverse problem, a structured grid is used to discretize the model domain. For the two-
320 dimensional cases, the number of grid blocks in x and y directions are n_x = 30 and n_y = 15 respectively
321 (See Figure R3). As a result, the total number of unknown K parameters is 450. For PCGA setup, we
322 use a truncation number of k=20 for a number of unknowns n=30*15, R=0.001*Id where Id is the
323 identity matrix, and δ=0.0001 for the finite difference interval. The specific storage was kept constant
324 in the inversion and the value is the same as in the forward simulation, i.e., $S_s = 10^{-4}$ m^{-1}. Figure 3
325 shows the results of the two-dimensional validation case. Figure 3a corresponds to the generated,
326 considered true, hydraulic conductivity field. Figure 3b is the inverted hydraulic conductivity field
327 using a classical hydraulic tomography that used similar covariance information as in the generation
328 of the random field. Figure 3d shows the interpreted hydraulic conductivity from flowmeter analysis.
329 Figures 3c, 3e and 3f show the inverted hydraulic conductivity by integrating flowmeter
330 interpretations into prior information of the inversion; Figure 3c used the interpreted hydraulic
331 conductivity in Figure 3d to initialize only the parameter; Figure 3e used the interpreted hydraulic
332 conductivity in Figure 3d to initialize both the parameter and the covariance matrix which remained
333 constant during inversion iterations; Figure 3f used the interpreted hydraulic conductivity in Figure 3d

to initialize both the parameter and the covariance matrix which was updated during inversion iterations.

The flowmeter interpretation allows the detection of the main layers in the system (Figure 3d) while the attempt of an inversion using only pumping tests data couldn't assess the vertical profiles of hydraulic conductivity (Figure 3b). Figure 3c, 3e and 3f show better K estimates. Flowmeter data clearly carry non-redundant information on the vertical hydraulic conductivity profiles along the wells. By only using the obtained hydraulic conductivity map from flowmeter interpretation as an initial guess, the inverted conductivity already contains vertical profile information and show different layers (Figure 3c). The inverted hydraulic conductivity shown in (Figure 3e) is also representative of a layered system but clearly not better than the inverted hydraulic conductivity shown in (Figure 3c). On the contrary, when the nested covariance has the freedom to update through inversion iterations, the best parameter estimate was obtained compared to all other configurations (Figure 3f).

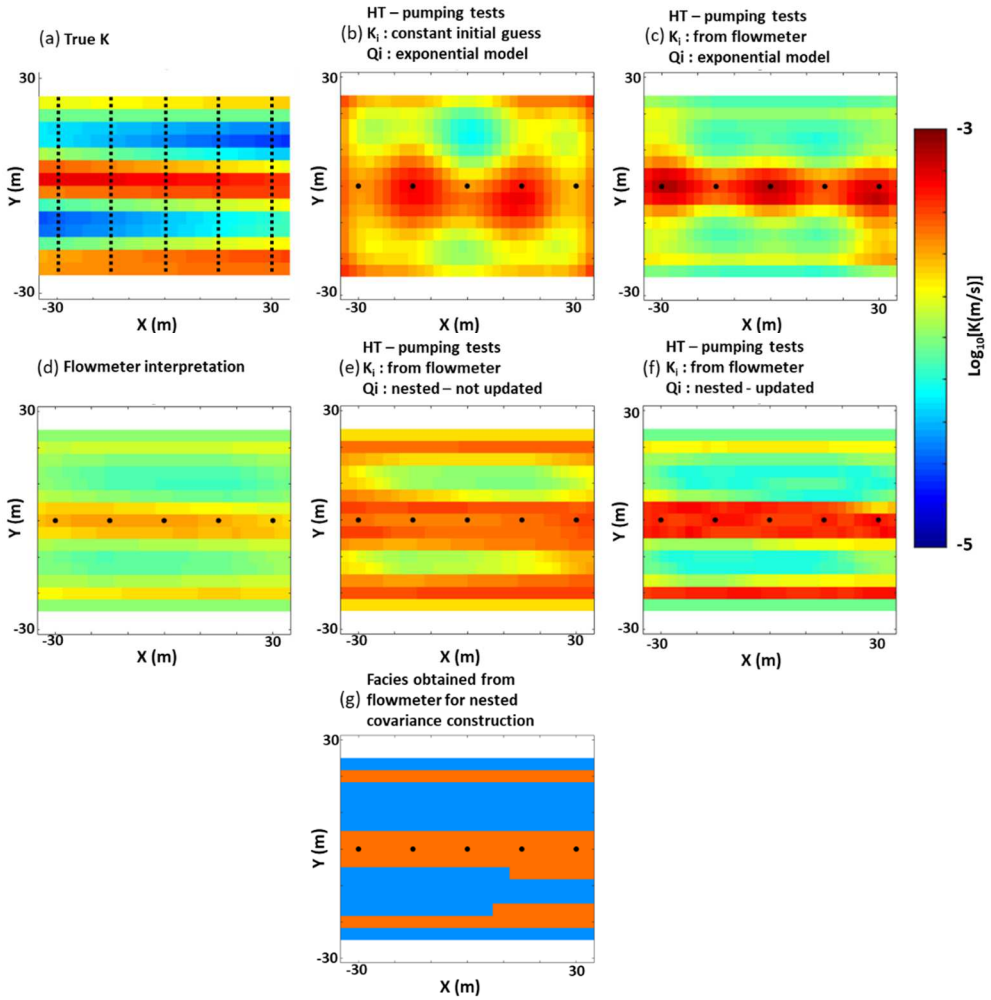

Figure 3*: Two-dimensional validation case – results of HT using different prior information. a) true hydraulic conductivity, d) interpreted hydraulic conductivity from flowmeter tests, b, c, e and f are inverted hydraulic conductivities using different prior models. K_i and Q_i correspond to the initial hydraulic conductivity and initial covariance matrix respectively, g) is the constructed facies from flowmeter analyses to use in order to construct the nested covariance.*

Figure 4 shows a scatter plot of true hydraulic conductivity and estimated hydraulic conductivity shown in Figure 3. In each scatter plot we plot a linear model of data fitting (red dashed line) and calculated the coefficient of determination, i.e., R^2 shown in Figure 4. The solid line is the first bisector line of y=x. Figures 4a and 4b present results of using pumping tests and an exponential covariance model for inversion. The difference is that in Figure 4a the initial guess of hydraulic conductivity was assumed constant while in Figure 4b the hydraulic conductivity distribution constructed by interpolating measured flowmeter profiles was used as the initial model. When the

flowmeter data are integrated, the inverted hydraulic conductivities represent the true model better (R^2 of Figure 4b is lower than that of Figure 4a). On the other hand, Figure 4c confirms that the flowmeter data can capture the true K distribution to some extent indicated by the strong linear trend and high value of R^2. However, the variance of the hydraulic conductivity estimates seems underestimated. The improved hydraulic conductivity estimation is obtained when flowmeter data are used to construct both the initial model and the covariance model (Figure 4d). Comparing results shown in Figures 4d and 4e indicates that allowing the update of the nested covariance improves the estimation considerably.

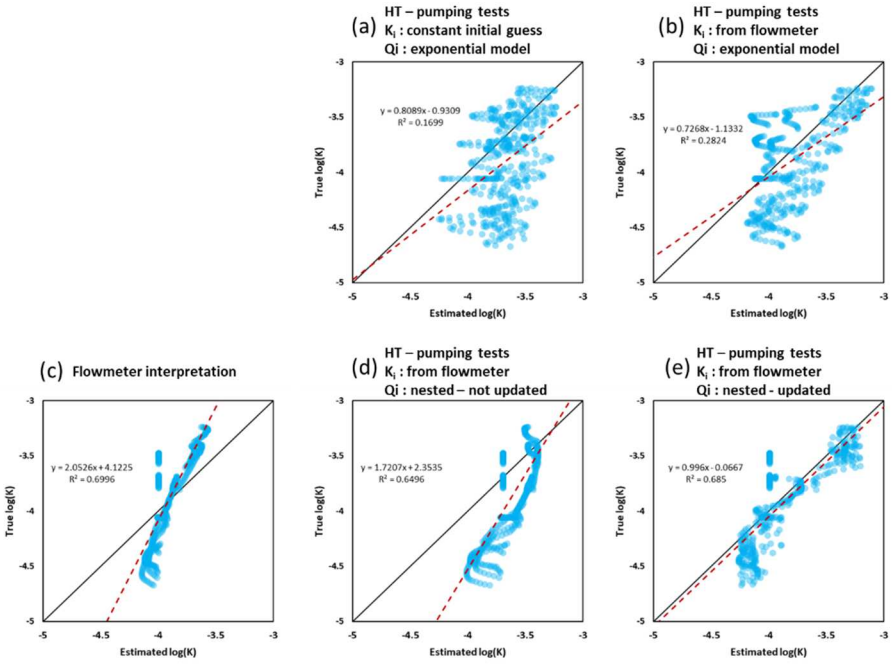

Figure 4*: Scatterplots of true hydraulic conductivity versus estimated hydraulic conductivity for the different cases of the two-dimensional synthetic case. c) scatter plot of true K versus interpreted K from flowmeter. a, b, d and e are scatter plots of true K versus inverted K using different prior models.*

3.2. 3D synthetic case

We extend the approach to a three-dimensional synthetic case and try to show if flowmeter data can provide the vertical information for a 3D aquifer characterization instead of packer tests. Similar to the simplified two-dimensional case, we use a three-dimensional random field generator (Rass et al. 2019) to generate a three-dimensional synthetic hydraulic conductivity map using the following parameters (Correlation function: exponential, standard deviation = 1.5, L_x=100 m, L_y=100 m and L_z=

377 5 m). Such parameters provide a hydraulic conductivity map that is representative of a multilayered
378 system. The dimensions of the inverted domain are length=70 m, width=70 m and height=30 m; the
379 lateral dimensions of the buffer area are length=700 m and width=700 m; the buffer was not extended
380 in the vertical direction. The outer boundaries are set to constant zero hydraulic head while the upper
381 and lower boundaries (top and bottom) are set to no flow condition. The initial condition is set to zero
382 hydraulic head in the whole domain. The specific storage is assumed constant and a value of $S_s = 10^{-4}$
383 m^{-1} was used.
384 As for the two-dimensional case, we simulate flowmeter and cross-hole datasets by modelling explicit
385 wells and point source pump (the point source in the top for the flowmeter simulation and in the
386 middle for cross-hole tests simulations). Extra fine meshes are adopted to discretize the well domain
387 (Figure R3). See Figure R2 in supplementary material for an example of simulated flowmeter
388 measurements for the 3D case. Five cross-hole pumping tests data are simulated and considered as the
389 'data' for the inversions. The location of selected wells is indicated in Figure S4. As for the 2D cases,
390 the total number of observations for the 3D cases is 100. The flowmeter data are interpreted and the
391 hydraulic conductivity profiles are then interpolated using a triangular-base trilinear interpolation to
392 fill the area between the wells. The rest of the inversion domain where the linear interpolation cannot
393 be evaluated, we use a nearest neighbors' extrapolation.
394 We construct a nested covariance using the interpreted flowmeter map as described for the two-
395 dimensional case. In the inverse problem, a structured grid is used to discretize the model domain. For
396 the three-dimensional cases, the number of grid blocks in x, y and z directions are nx = 20, ny = 20, nz
397 = 8 respectively (See Figure R3). For PCGA setup, we use a truncation number of k=30 for a number
398 of unknowns n=20*20*8, R=0.001*Id where Id is the identity matrix and δ=0.0001 for the finite
399 difference interval. The specific storage was kept constant ($S_s = 10^{-4}$ m^{-1}) in the inversion and we
400 focus on the characterization of K fields.
401 Figure 5 shows the results of the three-dimensional validation case. Figure 5c corresponds to the
402 generated, considered true, hydraulic conductivity field. Figure 5a is the inverted hydraulic
403 conductivity field using a classical hydraulic tomography that used same covariance information as in
404 the random field generation. Figure 5b shows the interpreted hydraulic conductivity from flowmeter

405 analysis. Figures 5d and 5e show the inverted hydraulic conductivity by integrating flowmeter
406 interpretations into prior information of the inversion; Figure 5d used the interpreted hydraulic
407 conductivity in Figure 5b to initialize only the parameter; Figure 5e used the interpreted hydraulic
408 conductivity in Figure 5b to initialize both the parameter and the covariance matrix which was
409 updated during inversion iterations.
410 The results of the 3D validation case agree with the observed results of the 2D validation case. The
411 flowmeter interpretation allows vaguely the detection of the main layers in the system (Figure 5b)
412 while the attempt of an inversion using only pumping tests data couldn't assess the vertical profiles of
413 hydraulic conductivity (Figure 5a). Figures 5d and 5e show better characterization in the vertical
414 profiles due to non-redundant added information brought by flowmeter data. Using the flowmeter's
415 interpreted hydraulic conductivity as an initial guess in the inversion already improves considerably
416 the results (Figure 5d). Also, as seen in the 2D validation case, the best K estimate was obtained when
417 flowmeter interpretation was used to initialize both the parameter and the covariance matrix (Figure
418 5e).

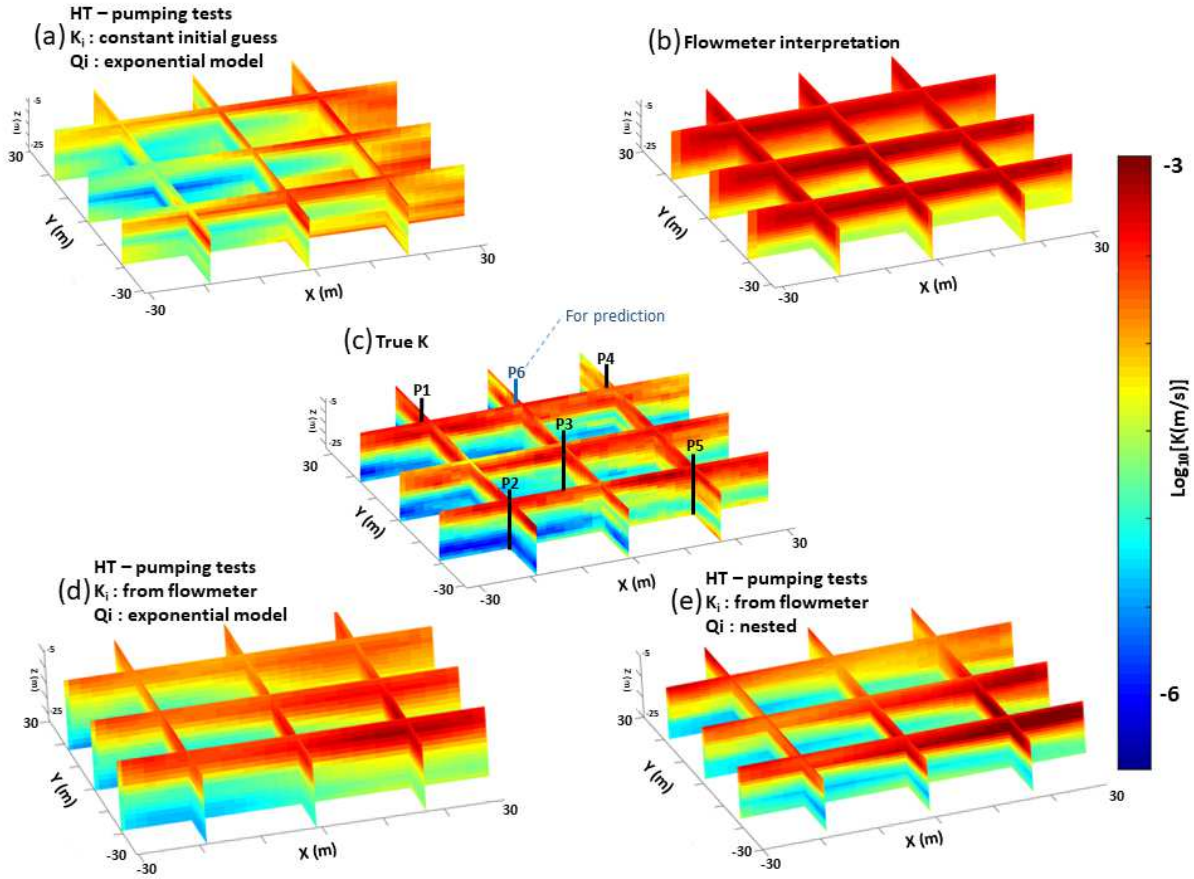

Figure 5*: Three-dimensional validation case - results of HT using different prior information; b) interpreted hydraulic conductivity from flowmeter tests, c) true hydraulic conductivity, a, d and e are inverted hydraulic conductivities using different prior models. K_i and Q_i correspond to the initial hydraulic conductivity and initial covariance matrix respectively.*

These results obtained with the 3D synthetic case are similar to the ones obtained with the 2D synthetic case, and thus confirm that adding flowmeter information allows improving the hydraulic permeability field. This conclusion is consistent with the fact that flux, in addition to hydraulic head measurements, enhance K values estimate (Yeh et al. (2011, 2015a, 2015b), Mao et al. (2013a, 2013b), Tso et al. 2016).

To better evaluate the quality of the estimated hydraulic conductivity field, we simulate a transient pumping test in well P6 (see Figure 5c) using this inverted hydraulic conductivity map and compare the simulated drawdowns to the simulated drawdowns obtained with the true hydraulic conductivity field (see Figure 6).

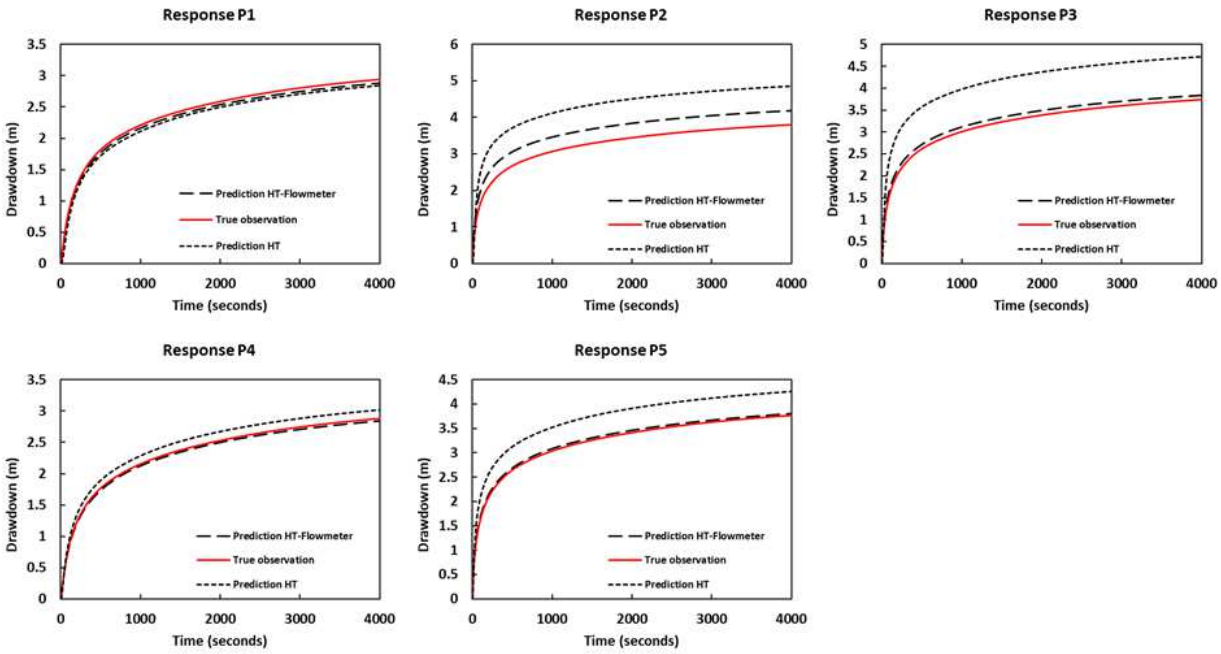

Figure 6*: Hydraulic head response to simulated pumping tests in the new added well P6. Solid red, dotted and dashed black curves correspond to the simulated drawdowns using respectively the true conductivity, the hydraulic conductivity map obtained from hydraulic tomography and the hydraulic conductivity map obtained from the hydraulic tomography conditioned by flowmeter analysis data.*

Figure 6 compares different drawdowns obtained on 5 boreholes in response to a pumping test in the new added prediction well P6. The drawdowns were simulated by using different hydraulic conductivity fields; the curves represented by solid red lines correspond to simulated drawdowns using true hydraulic conductivity; the curves represented by dotted black lines correspond to simulated drawdowns using inverted hydraulic conductivity obtained from hydraulic tomography using other pumping tests observation data (Figure 5a); the curves represented by dashed black lines correspond to simulated drawdowns using inverted hydraulic conductivity obtained from hydraulic tomography using other pumping tests observation data and conditioned by flowmeter data (Figure 5e). The results clearly show that the dashed lines (HT + flowmeter data) are closer to the solid red lines (true drawdown) compared to the dotted lines (classical HT). Such observation confirms that incorporating flowmeter data in the hydraulic tomography leads to better K estimates.

We also show a scatter plot of true hydraulic conductivity and estimated hydraulic conductivity in Figure 7. Each scatter plot has a linear model of data fitting represented by a red dashed line with a

linear regression expression and a coefficient of determination. The solid line is the first bisector line of y=x. Figure 7a shows the result of using pumping tests and an exponential covariance model. Figure 7b presents the result of hydraulic conductivity comparison based on flowmeter interpretation. The small bias toward high absolute values of hydraulic conductivities indicates that the effective hydraulic conductivity is overestimated by the interpolation of flowmeter profiles. When the interpreted hydraulic conductivity distribution from flowmeter is used as initial guess for the inversion, we observe that the characterization of hydraulic conductivity becomes considerably better (compare Figure 7c to Figure 7a). The incorporation of multiscale heterogeneity with the nested covariance model generates a different representation, but the hydraulic conductivity estimates is considerably improved as well (Figure 7d). This demonstrates the importance of integrating flowmeter data.

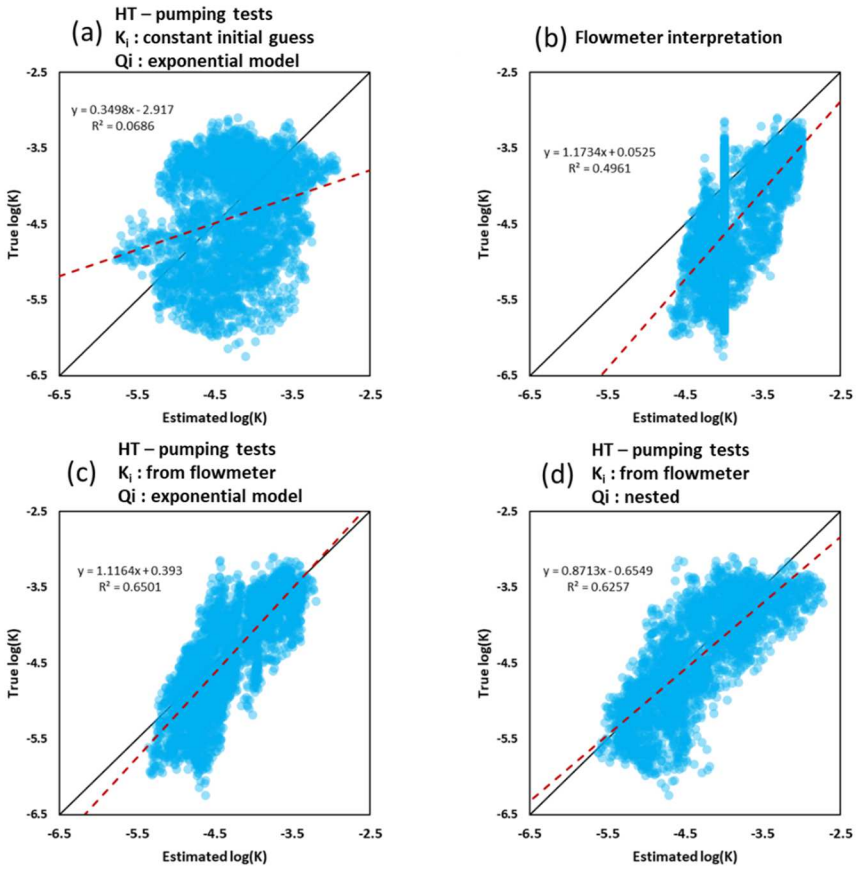

***Figure 7**: Two-dimensional validation case – scatterplots of true hydraulic conductivity versus estimated hydraulic conductivity for the different cases of the two-dimensional synthetic case. b) scatter plot of true K versus interpreted K from flowmeter. a, c and d are scatter plots of true K versus inverted K using different prior models.*

4. Application

In this section, the approach is applied to an experimental field site on the basis of real field data. The experimental site is located in Southern France, 20 km northeast of Montpellier (Figure 8a). The site's aquifer is composed of mollusc shells of late Burdigalian. The deposit is a dune system constructed during Miocene's tidal currents. Within the experimental site, 13 vertical wells were drilled in a square of 50 m by 50 m in which full-diameter cores were obtained in borehole P6, P8 and P12 (Figure 8b). The wells have a depth of 30m and are fully-penetrating wells, since they crosscut the whole late Burdigalian, down to the roof of the mid Burdigalian which presents a very low permeability. The hydraulic conductivity measured using 330 one-inch diameter cores plugged from the full-diameter cores spans four orders of magnitude (10^{-8} to 10^{-4}). The preliminary analysis of hydrodynamic response to pumping test and slug tests (Wang et al., 2019) showed a pretty high lateral heterogeneity of the hydraulic conductivity field. Besides, both the well logs and laboratory measurements on cores, showed that the spatial distribution of the hydraulic conductivity field is constrained by a multilayered system (Figure 8c).

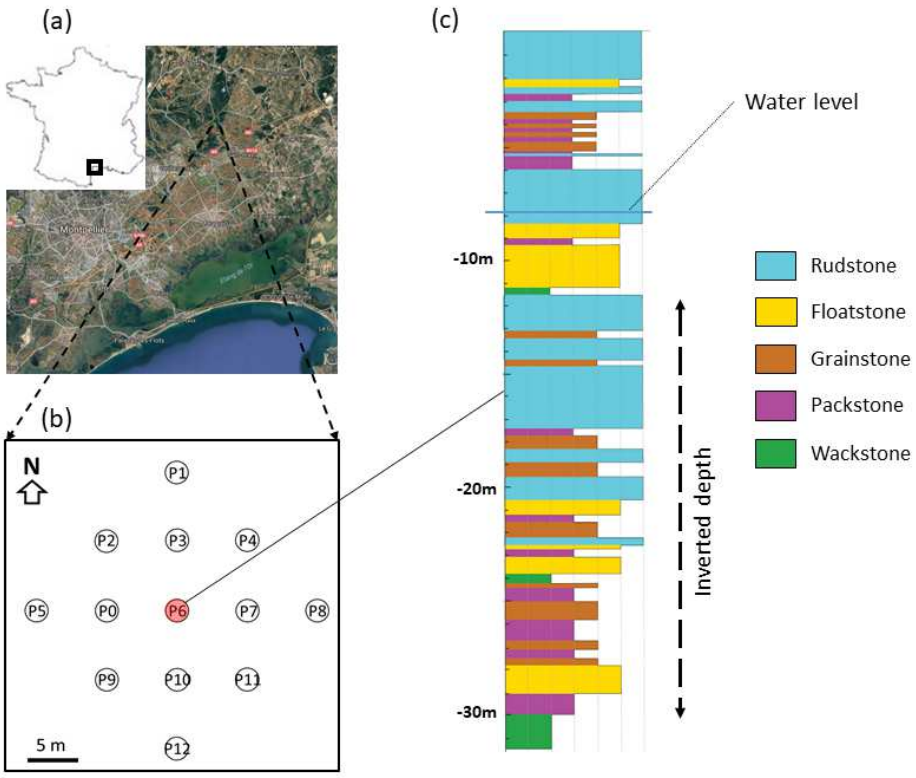

***Figure 8**: Experimental site composed of a multilayered system. a) geo-localization map, b) well pattern, c) log of P6 obtained from the core analysis.*

4.1. Flowmeter implementation and analysis

A series of spinner flowmeter tests are performed in the experimental site. The flowmeter tests are performed in each well. As described in the methodology, the flow log is obtained in a well subject to a pumping where the pump is positioned close to the surface. We also point out that the pump needs to remain under water and, depending on the generated drawdown, the investigated depth will be limited. To maximize the investigated depth, a small pumping flow rate was used. A series of flowmeter sweeps are performed inside a PVC with static water in order to realize the tool calibration of spin-velocity conversion. The log of flow rate can be obtained by taking into consideration the well diameter changes along the depth. An example of flowmeter measurements and interpretation for hydraulic conductivity distribution may be found in the supplementary material (Figure S3).

Considering that the total pumping flow rate comes under the pump, we can estimate the hydraulic conductivity log of the well as a function of the flow rate contribution of the different layers, once the effective hydraulic conductivity of the investigated depth of the aquifer is determined.

With the estimated hydraulic conductivity logs from the different wells, we fill the remaining space between them by interpolation, assuming that the distribution of the hydraulic properties in layers is continuous and correlated. A 3D hydraulic conductivity field is obtained.

4.2. Pumping tests data

13 pumping tests were performed in our experimental site during summer 2016. During each test, the transient responses are measured in all the wells for all the tests. The pumping tests were long enough to reach a pseudo-steady state response. We randomly choose 5 cross hole pumping tests to use as observations for the following application. Different times from early and middle parts of the response were sampled and used as the HT observations. We didn't sample from late time to avoid any instability that may come from the biased modelling of the uncertain regional heterogeneity and boundary conditions. From the well test analysis, the estimated effective permeability and specific storage of the test site are K_{eff} = 1.34e-4 m.s^{-1} and Ss = 2.65e-5 m^{-1}, which are used in the inversions.

4.3. Hydraulic tomography

The dimensions of the inverted domain are length=50 m, width=50 m and height=20 m; the dimensions of the buffer area are length=200 m, width=200 m and height=20 m. The outer boundaries

511 are set to constant hydraulic head h_0=25 m while the upper and lower boundaries (top and bottom) are
512 set to no flow condition. The initial condition is set to a constant hydraulic head h_0=25 m in the whole
513 domain. A covariance matrix is constructed using the hydraulic conductivity field. In fact, a nested
514 covariance function for multiscale heterogeneity is used in order to perform the inversion. It allows to
515 incorporate geological information to constrain the results (Zha et al. 2017). The nested covariance
516 matrix constructed based on flowmeter data interpolation can be found in Figure S5. The statistical
517 parameter used for the generating the covariance is provided in Table S2. Different facies are
518 determined and, in each facies, a correlation is defined. The main objective is not to perfectly
519 reproduce the drawdown responses, but to obtain a more realistic hydraulic property distribution with
520 a good fitting of the observed drawdowns. The initial guess is constructed from flowmeter interpreted
521 hydraulic conductivity field. A similar interpolation method as adopted in the synthetic inversion is
522 used to interpolate the flowmeter data. The covariance matrix is built accordingly to flowmeter results;
523 layers information is prioritized. The covariance is a result of a sum of different covariance matrices,
524 one defines the layers, another represents the variance and correlation length inside each layer and the
525 last one defines the variance and the correlation length of the whole domain.
526 For the experimental field case, we performed two inversion runs, the first one by a classical
527 hydraulic tomography approach and we used only observation from the pumping tests, while in the
528 second run, flowmeter interpretations were used to initialize the parameter and the covariance matrix.
529 Figure 7 shows the inverted hydraulic conductivity for both cases; Figure 7a corresponds to the
530 inverted hydraulic conductivity field with classical hydraulic tomography while Figure 7b
531 corresponds to the inverted hydraulic conductivity field with hydraulic tomography conditioned by
532 flowmeter data; Figures 7c and 7d are scatter plots of observations (hydraulic head measurements)
533 data fitting obtained using respectively results from Figure 7a and 7b.

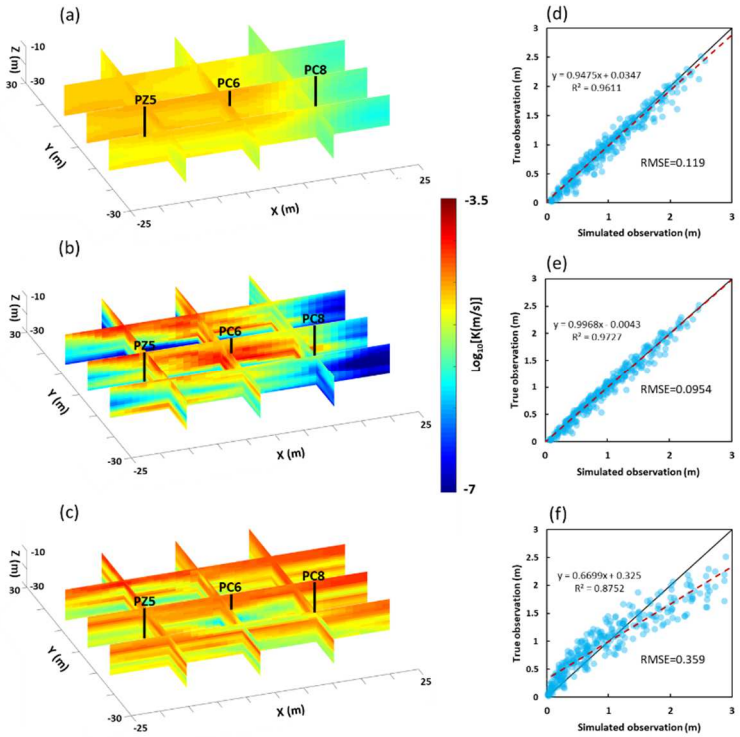

Figure 9: *Inverted hydraulic conductivity map and observation data fitting results from hydraulic tomography of real-case experimental site. a) inverted hydraulic conductivity map obtained from classical HT, b) inverted hydraulic conductivity map obtained from HT conditioned by flowmeter data, c) hydraulic conductivity map obtained from flowmeter interpretation, d) data fitting for classical HT results, e) data fitting for HT conditioned by flowmeter data, f) data fitting for flowmeter interpretation.*

5. Discussion

Incorporating flowmeter data into hydraulic tomography allows to obtain a better K estimate in the synthetic validation cases. For the 2D validation case, the results (see Figure 3) show that initializing the parameter and the covariance matrix with flowmeter interpretation data provides better K estimates. The initial parameter value can play an important role on converging to a different K estimate solution. Such an effect can be observed on the inverted hydraulic conductivity when flowmeter estimate was used to initialize the parameter (Figure 3c). On the other hand, the initial covariance matrix can also contain layers' information by correlating the cells that belong to the same layer. However, the correlation constraint can be strong on the K estimate especially when the covariance remains unchanged and equal to the initial (Figure 3e). The covariance of unknown

551 parameter can be updated to derive the residual covariance, the continuous updating of residual
552 covariance allows to correctly address the uncertainty and enhance convergence of the inverse
553 solution (Zha et al. 2018) which can be confirmed with the results in Figure 3f.
554 The approach of integrating flowmeter data was also tested using synthetic case in three dimensions
555 and results (see Figure 5) are in total agreement with the 2D case observations. For this case, we also
556 showed the quality of the result by simulating drawdown curves in a prediction well (which was not
557 included in observation wells) using the inverted hydraulic conductivity field and compared them with
558 the true observed drawdown (see Figure 6). It clearly shows how flowmeter data adds a non-
559 redundant vertical profile information and, thus, enhance considerably the K estimates. In the present
560 study, we focused on reconstructing K distributions by keeping S_s as a constant. Although previous
561 studies have shown that the selection of S_s value may impact the K estimates (Castagna et al., 2011;
562 Zhao et al., 2021), our interpretation of field site single-hole and cross-hole pumping tests did not
563 indicate a strong variation of S_s. For this reason, we think the treatment is reasonable. However, in the
564 future, we attempt to perform a full inversion to simultaneously estimate the spatial distribution of
565 both K and S_s. These would require more pumping test data points to be sampled and used in the
566 inversion as the inclusion of S_s distribution would double the number of unknown parameters, which
567 increases drastically the underdetermined-ness of the inversion problem.
568 Figure 9 summarizes the results of the approach applied to a real field case. The two inverted
569 hydraulic conductivity fields are totally different from each other while their data fitting are quite
570 similar. K estimates obtained from HT conditioned by flowmeter data exhibits a multilayered system
571 with more geological realism comparing to K estimates obtained from classical HT without any
572 additional profile information. The same layering system has been observed in other measurements
573 (core analysis, logs, permeameter measurements, etc.).
574 The data fitting in both inversions is relatively similar (RMSE = 0.0912 for HT using pumping tests
575 data and RMSE = 0.0874 for HT using pumping tests and flowmeter data). However, the prediction of
576 transient drawdowns becomes significantly better using K estimate obtained with the incorporation of
577 flux measurements data. For further validation, we sampled hydraulic conductivity values from
578 inversion results and we compared them to some available permeameter measurements at the same

579 locations. Within the 13 wells available in the experimental site, three (PC6, PC8 and PC12) were
580 cored. Cores allowed to obtain a permeability log from laboratory permeameter measurements along
581 the wells. Figure 8 shows a comparison of extracted conductivity from THT results and laboratory
582 permeability measurements (converted into hydraulic conductivity using water density ρ=1000 kg m^{-3},
583 water viscosity μ=0.001 kg m^{-1} s^{-1} and gravity acceleration g=9.81 m s^{-2}) of plugs on the cored wells
584 as well as the flowmeter interpreted hydraulic conductivity.

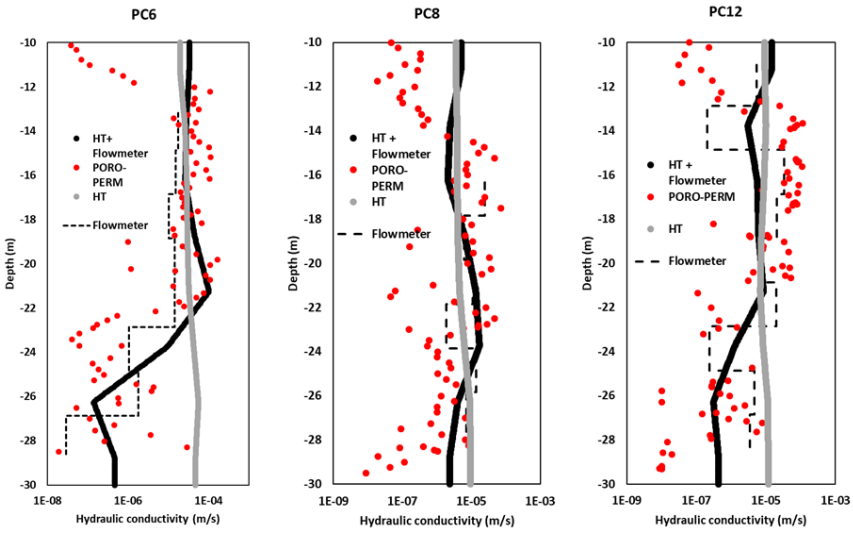

585

586 ***Figure 10****: Hydraulic conductivity profiles for wells PC6, PC8 and PC12 of the experimental site.*
587 *Red dots are laboratory measurements. Grey solid line is extracted from THT results. Black solid line*
588 *is extracted from THT integrating flowmeter analysis data results. Dashed line is from flowmeter*
589 *interpretation.*

590 Figure 10 strengthen the fact that flowmeter data enhance HT results, especially in the vertical profiles
591 of the hydraulic conductivity estimates. Flowmeter conditioning data allows the K estimate to get
592 closer to the measured permeability from the plugs of the cored wells. Hydraulic conductivity
593 profiles in the wells obtained from transient hydraulic tomography (Figure 10, grey solid line), show
594 that normal pumping tests do not contain vertical information about the aquifer's hydraulic properties;
595 the hydraulic conductivity profiles are similar to a result of a 2D THT extruded into the third
596 dimension (depth averaged values).

Our work is in agreement with other previous works in terms of how flux measurements enhance hydraulic tomography results. The work of Li et al. (2008) showed that inverting both steady state hydraulic head measurements and flux measurements data leads to better hydraulic conductivity estimates. They used both data in the inverse process as conditioning observations. However, in this work, only transient hydraulic head measurements are used to condition the inversion and flowmeter tests data are used to initialize the prior inputs of the inversion. Our results show that incorporating flowmeter data in the initial parameter and the prior covariance matrix may be sufficient to enhance considerably the K estimates. Zha et al. (2014) and Tso et al. (2016) also worked on combining flux measurements with pumping tests data. Zha et al. (2014) inverted synthetic case in 2D by using normal pumping tests and used lateral fluxes as an additional data to strengthen the result and Tso et al. (2016) extended it to 3D by using the same observation datasets. They both showed that flux data improves estimates resolution of HT analysis. The difference between the two studies is the dimension and the fact that Zha et al. (2014) used it to characterize a discrete fracture network while Tso et al. (2016) investigated a porous media instead. However, both studies were not tested on any real case study.

6. Summary and conclusions

In this study, we performed a transient hydraulic tomography of cross-hole pumping tests by integrating flowmeter data in prior inputs on an experimental site and managed a 3D imaging of the aquifer system that was coherent with geological observations and existing permeability measurements. We used flowmeter data as source of the vertical information additional to pumping tests that provides the lateral information. In order to incorporate the vertical data into hydraulic tomography, flowmeter tests are interpreted separately to obtain a prior K estimate which was used to initialize the parameter and the covariance matrix. While, the pumping tests observations were used to condition the inversion convergence process. Using different initial parameters and initial covariance matrices showed that the prior inputs of the inversion are important and can modify the result considerably. Also, the non-packer pumping tests do not contain vertical information: the inverted hydraulic conductivity using only pumping tests was generally constant along the vertical profile. The

integration of vertical hydrogeological information obtained from flowmeter surveys and horizontal information from cross-hole pumping tests allow a 3D transient hydraulic tomographic (THT) characterization of sedimentary layered rocks. Flowmeter data are a non-redundant information and different data other than flowmeter could also be used to better define the variations of vertical hydraulic conductivity such as laboratory measurements on cored wells or classical logs that are able to be converted into relative conductivity profiles.

Acknowledgements

The authors thank TOTALENERGIES (R&D in Pau, France) for supporting the present study and for granting permission to publish this paper. X.W is supported by the National Key Research and Development Program of China (No. 2020YFC1808300) and National Natural Science Foundation of China (No. 42102300).

References

Berg, S. J., and W. A. Illman (2011), Three-dimensional transient hydraulic tomography in a highly heterogeneous glaciofluvial aquifer-aquitard system, Water Resour. Res., 47, W10507, doi:10.1029/2011WR010616.

Bohling, G. C., Butler Jr., J. J., Zhan, X., and Knoll, M. D. (2007), A field assessment of the value of steady shape hydraulic tomography for characterization of aquifer heterogeneities, Water Resour. Res., 43, W05430, doi:10.1029/2006WR004932.

Bohling, G. C., Zhan, X., Butler, J. J., and Zheng, L., Steady shape analysis of tomographic pumping tests for characterization of aquifer heterogeneities, Water Resour. Res., 38(12), 1324, doi:10.1029/2001WR001176, 2002.

Bohling, G.C. and Butler, J.J., Jr. (2010), Inherent Limitations of Hydraulic Tomography. Groundwater, 48: 809-824. https://doi.org/10.1111/j.1745-6584.2010.00757.x

Brauchler, R., R. Hu, L. Hu, S. Jimenez, P. Bayer, P. Dietrich, and T. Ptak (2013), Rapid field application of hydraulic tomography for resolving aquifer heterogeneity in unconsolidated sediments, Water Resour. Res., 49, 2013–2024, doi:10.1002/wrcr.20181.

Brauchler, R., R. Hu, P. Dietrich, and M. Sauter (2011), A field assessment of high-resolution aquifer characterization based on hydraulic travel time and hydraulic attenuation tomography, Water Resour. Res., 47, W03503, doi:10.1029/2010WR009635.

Butler, J. J., McElwee, C. D., and Bohling, G. C. (1999), Pumping tests in networks of multilevel sampling wells: Motivation and methodology, Water Resour. Res., 35(11), 3553– 3560, doi:10.1029/1999WR900231.

Cardiff, M., Barrash, W., and Kitanidis, P. K. (2012), A field proof-of-concept of aquifer imaging using 3-D transient hydraulic tomography with modular, temporarily-emplaced equipment, Water Resour. Res., 48, W05531, doi:10.1029/2011WR011704.

Cardiff, M., W. Barrash, P. K. Kitanidis, B. Malama, A. Revil, S. Straface, and E. Rizzo (2009), A potential-based inversion of unconfined steadystate hydraulic tomography, Ground Water, 47(2), 259–270, doi:10.1111/j.1745-6584.2008.00541.x

Chen, J.S., S. Hubbard, and Y. Rubin. 2001. Estimating thehydraulic conductivity at the South Oyster Site from geo-physical tomographic data using Bayesian techniquesbased on the normal linear regression model. Water Re-sources Research 37, no. 6: 1603–1613

COMSOL AB (2018), Subsurface Flow Module User's Guide, COMSOL Multiphysics v. 5.4, COMSOL AB, Stockholm, Sweden

Cooper, H. H., and Jacob, C. E. (1946), A generalized graphical method for evaluating formation constants and summarizing well-field history, Eos Trans. AGU, 27(4), 526– 534, doi:10.1029/TR027i004p00526

Day-Lewis, F.D., Johnson, C.D., Paillet, F.L. and Halford, K.J. (2011), A Computer Program for Flow-Log Analysis of Single Holes (FLASH). Groundwater, 49: 926-931. https://doi.org/10.1111/j.1745-6584.2011.00798.x

De Clercq T., A. Jardani, P. Fischer, L. Thanberger, T.M. Vu, D. Pitaval, J.-M. Côme, P. Begassat. 2020. The use of electrical resistivity tomograms as a parameterization for the hydraulic characterization of a contaminated aquifer. Journal of Hydrology 587: 124986.

676 Fienen, M.N., P.K. Kitanidis, D. Watson, and P. Jardine. 2004.An application of Bayesian inverse
677 methods to vertical de-convolution of hydraulic conductivity in a heterogeneousaquifer at Oak Ridge
678 National Laboratory. MathematicalGeology 36, no. 1: 101–126.

679 Fischer P., Jardani A., Jourde H., Hydraulic tomography in coupled discrete-continuum concept to
680 image hydraulic properties of a fractured and karstified aquifer (Lez aquifer, France) Adv. Water
681 Resour., 137 (2020), p. 103523, 10.1016/j.advwatres.2020.103523

682 Gottlieb, J., and P. Dietrich. 1995. Identification of the permeability distribution in soil by hydraulic
683 tomography. InverseProblems 11, no. 2: 353–360.

684 Hubbard S.S., Rubin Y. (2005) Introduction to Hydrogeophysics. In: Rubin Y., Hubbard S.S. (eds)
685 Hydrogeophysics. Water Science and Technology Library, vol 50. Springer, Dordrecht.
686 https://doi.org/10.1007/1-4020-3102-5_1

687 Illman, W. A., Zhu, J., Craig, A. J., and Yin, D. (2010), Comparison of aquifer characterization
688 approaches through steady state groundwater model validation: A controlled laboratory sandbox
689 study, Water Resour. Res., 46, W04502, doi:10.1029/2009WR007745.

690 Illman, W.A., X. Liu, and A. Craig. 2007. Steady-state hydraulictomography in a laboratory aquifer
691 with deterministic het-erogeneity: Multi-method and multiscale validation ofhydraulic conductivity
692 tomograms, Journal of Hydrology341, no. 3–4: 222–234

693 Javandel, I., and P.A. Witherspoon. 1969. A method of analyzing transient fluid flow in multilayered
694 aquifer. WaterResources Research 5, no. 4: 856–869.

695 Kabala, Z. J. (1994), Measuring distributions of hydraulic conductivity and specific storativity by the
696 double flowmeter test, Water Resour. Res., 30(3), 685– 690, doi:10.1029/93WR03104

697 Kitanidis, P. K., and Lee, J. (2014), Principal Component Geostatistical Approach for large
698 dimensional inverse problems, Water Resour. Res., 50, 5428– 5443, doi:10.1002/2013WR014630.

699 Kitanidis, P.K. 1995. Quasi-linear geostatistical theory for inversing. Water Resources Research 31,
700 no. 10: 2411–2419.

701 Klepikova, M. V., Le Borgne, T.., Bour, O., and de Dreuzy, J.-R. (2013), Inverse modeling of flow
702 tomography experiments in fractured media, Water Resour. Res., 49, 7255– 7265,
703 doi:10.1002/2013WR013722.

704 Li, W., Englert, A., Cirpka, O.A. and Vereecken, H. (2008), Three-Dimensional Geostatistical
705 Inversion of Flowmeter and Pumping Test Data. Groundwater, 46: 193-201.
706 https://doi.org/10.1111/j.1745-6584.2007.00419.x

707 Liu, S., T.-C. J. Yeh, and R. Gardiner (2002), Effectiveness of hydraulic tomography: Sandbox
708 experiments, Water Resour. Res., 38(4), 1034, doi:10.1029/2001WR000338

709 Liu, X., Illman, W. A., Craig, A. J., Zhu, J., and Yeh, T.-C. J. (2007), Laboratory sandbox validation
710 of transient hydraulic tomography, Water Resour. Res., 43, W05404, doi:10.1029/2006WR005144.

711 Mao, D., T.-C. J. Yeh, L. Wan, C.-H. Lee, K.-C. Hsu, J.-C. Wen, and W. Lu (2013a), Cross-
712 correlation analysis and information content of observed heads during pumping in unconfined
713 aquifers, Water Resour. Res., 49, 713–731, doi:10.1002/wrcr.20066.

714 Mao, D., T.-C. J. Yeh, L. Wan, K.-C. Hsu, C.-H. Lee, and J.-C. Wen (2013b), Necessary conditions
715 for inverse modeling of flow through variably saturated porous media, Adv. Water Resour., 52, 50–61,
716 doi:10.1016/j.advwatres.2012.08.001.

717 Molz, F. J., Morin, R. H., Hess, A. E., Melville, J. G., and Güven, O. (1989), The Impeller Meter for
718 measuring aquifer permeability variations: Evaluation and comparison with other tests, Water Resour.
719 Res., 25(7), 1677– 1683, doi:10.1029/WR025i007p01677.

720 Molz, F.J., G.K. Boman, S.C. Young, and W.R. Waldrop. 1994. Borehole flowmeters: Field
721 application and data analysis.Journal of Hydrology 163, no. 4: 347–371.

722 Paillet, F. L. (1998), Flow modeling and permeability estimation using borehole flow logs in
723 heterogeneous fractured formations, Water Resour. Res., 34(5), 997– 1010, doi:10.1029/98WR00268.

724 Paillet, F.L. and Reese, R.S. (2000), Integrating Borehole Logs and Aquifer Tests in Aquifer
725 Characterization. Groundwater, 38: 713-725. https://doi.org/10.1111/j.1745-6584.2000.tb02707.x

726 Paul Constantine (2021). Random Field Simulation
727 (https://www.mathworks.com/matlabcentral/fileexchange/27613-random-field-simulation), MATLAB
728 Central File Exchange. Retrieved July 19, 2021.

729 Räss, L., Kolyukhin, D., Minakov, A. (2019). Efficient parallel random field generator for large 3-D
730 geophysical problems. Computers & Geosciences 131, 158-169

731 Rehfeldt, K. R., J. M. Boggs, and L. W. Gelhar (1992), Field study of dispersion in a heterogeneous
732 aquifer: 3. Geostatistical analysis of hydraulic conductivity, Water Resour. Res., 28(12), 3309–3324,
733 doi:10.1029/92WR01758.

734 Roubinet D., Irving J., Day-Lewis F.D., Development of a new semi-analytical model for cross-
735 borehole flow experiments in fractured media Adv. Water Res., 76 (2015), pp. 97-108,
736 10.1016/j.advwatres.2014.12.002

737 Soueid Ahmed, A., Zhou, J. Jardani, A., Revil, A., Dupont, J.P., Image-guided inversion in steady-
738 state hydraulic tomography Adv. Water Resour., 82 (2015), pp. 83-97,
739 10.1016/j.advwatres.2015.04.001.

740 Tamayo-Mas, M. Bianchi, M. Mansour Impact of model complexity and multi-scale data integration
741 on the estimation of hydrogeological parameters in a dual-porosity aquifer Hydrogeol. J., 26 (6)
742 (2018), pp. 1917-1933, 10.1007/s10040-018-1745-y

743 Theis, C. V. (1935), The relation between the lowering of the Piezometric surface and the rate and
744 duration of discharge of a well using ground-water storage, Eos Trans. AGU, 16(2), 519– 524,
745 doi:10.1029/TR016i002p00519.

746 Tso, M., C.-H., Zha, Y., J. Yeh, T.-C., and Wen, J.-C. (2016), The relative importance of head, flux,
747 and prior information in hydraulic tomography analysis, Water Resour. Res., 52, 3– 20,
748 doi:10.1002/2015WR017191.

749 Wang, X., Jourde, H., Aliouache, M., Massonnat, G., Characterization of horizontal transmissivity
750 anisotropy using cross-hole slug tests, J. Hydrol., 564 (2018), pp. 89-98,
751 10.1016/j.jhydrol.2018.06.068

752 Wen, J.-C., Chen, J.-L., Yeh, T.-C.J., Wang, Y.-L., Huang, S.-Y., Tian, Z. and Yu, C.-Y. (2020),
753 Redundant and Nonredundant Information for Model Calibration or Hydraulic Tomography.
754 Groundwater, 58: 79-92. https://doi.org/10.1111/gwat.12879

755 Williams, J., and F. Paillet (2002), Using flowmeter pulse tests to define hydraulic connections in the
756 subsurface: A fractured shale example, J. Hydrol., 265, 100–117.

757 Yeh, T.-C., M. Jin, and S. Hanna, An iterative stochastic inverse method: Conditional effective
758 transmissivity and hydraulic head fields, Water Resour. Res., 32(1), 85-92, 1996

759 Yeh, T.-C. J., and Liu, S. (2000), Hydraulic tomography: Development of a new aquifer test
760 method, Water Resour. Res., 36(8), 2095– 2105, doi:10.1029/2000WR900114.

761 Yeh, T.-C. J., D. Mao, L. Wan, C.-H. Lee, J.-C. Wen, and K.-C. Hsu (2011), Well Definedness, Scale
762 Consistency, and Resolution Issues in Groundwater Model Parameter Identification, Dep. of Hydrol.
763 and Water Resour., Univ. of Ariz., Tucson.

764 Yeh, T.-C. J., D. Mao, L. Wan, C.-H. Lee, J.-C. Wen, and K.-C. Hsu (2015b), Well definedness, scale
765 consistency, and resolution issues in groundwater model parameter identification, Water Sci. Eng.,
766 8(3), 175–194, doi:10.1016/j.wse.2015.08.002.

767 Yeh, T.-C. J., R. Khaleel, and K. C. Carroll (2015a), Flow Through Heterogeneous Geologic Media,
768 Cambridge Univ. Press, Cambridge, U. K.

769 Yeh, T.-C., Mas-Pla, J., Williams, T. M., and McCarthy, J. F. (1995), Observation and Three-
770 Dimensional Simulation of Chloride Plumes in a Sandy Aquifer Under Forced-Gradient Conditions,
771 Water Resour. Res., 31(9), 2141– 2157, doi:10.1029/95WR01947.

772 Zha, Y., T.-C. J. Yeh, D. Mao, J. Yang, and W. Lu (2014), Usefulness of flux measurements during
773 hydraulic tomographic survey for mapping hydraulic conductivity distribution in a fractured medium,
774 Adv. Water Resour., 71, 162–176, doi:10.1016/j.advwatres.2014.06.008.

775 Zha, Y., Yeh, T.-C. J., Illman, W. A., Zeng, W., Zhang, Y., Sun, F., et al. (2018). A reduced-order
776 successive linear estimator for geostatistical inversion and its application in hydraulic tomography.
777 Water Resources Research, 54, 1616– 1632. https://doi.org/10.1002/2017WR021884

778 Zha, Y., Yeh, T.-C.J., Illman, W.A., Tanaka, T., Bruines, P., Onoe, H., Saegusa, H., Mao, D.,
779 Takeuchi, S. and Wen, J.-C. (2016), An Application of Hydraulic Tomography to a Large-Scale
780 Fractured Granite Site, Mizunami, Japan. Groundwater, 54: 793-804.
781 https://doi.org/10.1111/gwat.12421

782 Zha, Y., Yeh, T.-C. J., Illman, W. A., Onoe, H., Mok, C. M. W., Wen, J.-C., Huang, S.-Y., and Wang,
783 W. (2017), Incorporating geologic information into hydraulic tomography: A general framework
784 based on geostatistical approach, Water Resour. Res., 53, 2850– 2876, doi:10.1002/2016WR019185.

785 Zhao, Z., and W. A. Illman (2017), On the Importance of Geological Data for Three-dimensional
786 Steady-State Hydraulic Tomography Analysis at a Highly Heterogeneous Aquifer-Aquitard System. J.
787 Hydrol., 544, 640– 657

788 Zhao,Z.,Illman,W.A.,Berg,S.J.,2016.On the importance of geological data for hy-draulic tomography
789 analysis: laboratory sandbox study. J.Hydrol.https://doi.org/10.1016/j.jhydrol.2016.08.061

790 Zheng, C. and Gorelick, S.M. (2003), Analysis of Solute Transport in Flow Fields Influenced by
791 Preferential Flowpaths at the Decimeter Scale. Groundwater, 41: 142-155.
792 https://doi.org/10.1111/j.1745-6584.2003.tb02578.x

793 Zhu, J., and T.-C. J. Yeh (2006), Analysis of hydraulic tomography using temporal moments of
794 drawdown recovery data, Water Resour. Res., 42, W02403, doi:10.1029/2005WR004309

795 Zhu, J., and Yeh, T.-C. J. (2005), Characterization of aquifer heterogeneity using transient hydraulic
796 tomography, Water Resour. Res., 41, W07028, doi:10.1029/2004WR003790.

797 Zlotnik, V.A., and B.R. Zurbuchen. 2003. Estimation of hydraulic conductivity from borehole
798 flowmeter tests consideringhead losses. Journal of Hydrology 281, no. 1–2: 115–128.